Carbon Trends 12 (2023) 100274

Contents lists available at ScienceDirect

Carbon Trends

journal homepage: www.elsevier.com/locate/cartre

Dielectric response and excitations of hydrogenated free-standing graphene

Maria Grazia Betti[a], Dario Marchiani[a], Andrea Tonelli[b], Marco Sbroscia[a], Elena Blundo[a], Marta De Luca[a], Antonio Polimeni[a], Riccardo Frisenda[a], Carlo Mariani[a,c], Samuel Jeong[d], Yoshikazu Ito[d], Nicola Cavani[b], Roberto Biagi[b,e], Peter N.O. Gillespie[e], Michael A. Hernandez Bertran[b,e], Miki Bonacci[e], Elisa Molinari[b,e], Valentina De Renzi[b,e,*], Deborah Prezzi[e,*]

[a] Physics Department, Sapienza University of Rome, Piazzale Aldo Moro 5, Rome 00185, Italy
[b] Physics, Informatics and Mathematics Department (FIM), University of Modena and Reggio Emilia, via G. Campi 213/a, Modena, 41125, Italy
[c] Istituto Nazionale di Fisica Nucleare (INFN), Piazzale Aldo Moro 5, Rome 00185, Italy
[d] Institute of Applied Physics, Graduate School of Pure and Applied Sciences, University of Tsukuba, Tsukuba 305-8573, Japan
[e] Istituto Nanoscienze (NANO-S3), Consiglio Nazionale delle Ricerche (CNR), via G. Campi 213/a, Modena 41125, Italy

ARTICLE INFO

Keywords:
Graphane
Nanoporous graphene
Hydrogen functionalization
Electron energy loss spectroscopy
Photoelectron spectroscopy
Density functional theory
GW-BSE calculations

ABSTRACT

The conversion of semimetallic suspended graphene (Gr) to a large-gap semiconducting phase is here realized by controlled adsorption of atomic hydrogen (deuterium) on free-standing nanoporous Gr veils. This approach allows to achieve a very clean and neat adsorption, overcoming any spurious influence associated to the presence of substrates. The effects of local rehybridization from sp^2 to sp^3 chemical bonding are investigated by combining X-ray photoelectron spectroscopy and high-resolution electron energy-loss spectroscopy (HREELS) with ab-initio based modelling. We find that the hydrogen adatoms on the C sites induce a stretching frequency, clearly identified in the vibrational spectra thanks to the use of the D isotope. Overall, the results are compatible with the predicted fingerprints of adsorption on both sides of Gr corresponding to the graphane configuration. Moreover, HREELS of the deuterated samples shows a sizeable opening of the optical band gap, i.e. 3.25 eV, consistent with the modified spectral density observed in the valence band photoemission. The results are in agreement with ab-initio calculations by *GW* and Bethe–Salpeter equation approaches, predicting a large quasiparticle gap opening and huge exciton binding energy.

1. Introduction

At variance with other two-dimensional (2D) materials, graphene exhibits an extreme chemical versatility, which has been extensively explored to build customizable properties and functionalities that are radically different from those of the parent material [1]. Hydrogenated graphene (H-Gr) is by far the simplest and one of the most studied chemical derivatives of graphene [2,3]. Depending on hydrogenation conditions and configurations, H-Gr has shown its potential for a wide range of different applications – from hydrogen storage [4–7] to catalysis [8,9], from opto-electronics [10–14] to biosensing [15–17]. In addition, intriguing optical phenomena, such as the realization of excitonic insulating phases [18,19] and optically controlled exciton traps [20], have been predicted for specific hydrogenation conditions.

The opening of a semiconducting gap, which results from the conversion from sp^2 to sp^3 hybridization of C atoms upon H adsorption, is crucial to many of these applications. Its value is highly tunable depending on the degree of hydrogenation, up to the insulating behaviour predicted [18,21] for fully hydrogenated graphene, i.e. graphane, where giant excitonic effects are also expected to dominate the dielectric response [18,22]. Small-gap tunability has been demonstrated at low coverage due to partial π-band disruption at the K point of the Brillouin zone [23,24], while evidences of large gaps have been recently reported in a few cases for highly hydrogenated samples [13,25,26]. However, the experimental measurement of the expected gap intrinsic to high-coverage and fully free-standing H-Gr has remained elusive so far.

Indeed, obtaining the ideal graphane arrangement [27,28], where a hydrogen atom is bound to each C atom of the 2D hexagonal scaffold, has proven to be an incredibly challenging task, and many observations are dominated by partial, inhomogeneous hydrogenation [29–31], with defects and open edges as key active hydrogen-C sites [12,32–34]. In addition, hydrogenation is often performed on supported samples [35–37], thus inhibiting the realization of a two-side hydrogenation and leading

* Corresponding authors.
E-mail addresses: vderenzi@unimore.it (V. De Renzi), deborah.prezzi@nano.cnr.it (D. Prezzi).

https://doi.org/10.1016/j.cartre.2023.100274
Received 1 June 2023; Accepted 2 June 2023

to remarkably different properties with respect to the ones intrinsic to a free-standing, fully hydrogenated graphene layer. For these reasons, most of the optical spectroscopic observations on H-Gr are attributed either to one-side hydrogenation of Gr on substrate [12,23,38] or to dot-like luminescence arising from unsaturated graphene patches [29,30].

In this work, we investigate the dielectric response and the corresponding optical band gap opening in high-quality samples of free-standing, hydrogenated Gr. In particular, we achieve a fine control on the evolution of the structural, electronic and optical properties in the conversion of pristine graphene to its hydrogenated phase by combining X-ray and UV photoelectron spectroscopies (XPS, UPS), high-resolution electron energy-loss (HREEL) experiments, and state-of-the-art ab-initio simulations. We focus on nanoporous graphene (NPG) samples, i.e., a compact, bicontinuous interconnected 3D graphene arrangement with one to few weakly interacting layers [39,40]. NPG represents an excellent testbed where to measure intrinsic properties induced by the hydrogenation process in view of the fully free-standing, high-quality nature of the specimens, with a very low density of defects. Notably, NPG recently demonstrated successful in supporting very high H/C adsorption rates, leading to the observation of a semiconducting phase [26] thermodynamically stable up to more than 600 °C [41]. The high temperature stability of the bond constitutes an important advantage in view of the use of the highest H isotope, tritium, bonded to the graphane mesh, as proposed for a futuristic neutrino detector [42–44].

Thanks to the use of atomic deuterium (D) [41], the characteristic D–C contribution in the vibrational spectra is identified here with HREEL spectroscopy and density-functional theory (DFT) simulations, allowing us to unequivocally pinpoint sp^3 bonds induced by the hydrogenation process while disregarding any contaminant effect. Moreover, the comparison between the photoemission spectral density and the dielectric response by means of electron scattering is exploited to support the realization of a large-gap semiconductor: upon deuteration, the presence of a valence band maximum (VBM) at about 3.50 eV below the Fermi level, as deduced by photoemission, is paired to the appearance of a transition onset at about 3.25 eV resulting from electron energy loss, which clearly confirms the transition from semimetallic suspended graphene to a semiconducting phase with a large optical band gap. These results are in agreement with predictions from ab-initio *GW* and Bethe–Salpeter equation (BSE) calculations, which show renormalized band gaps and large exciton binding energies with little variability with respect to the specific double-side H configuration.

2. Materials and methods

2.1. Sample preparation

NPG samples were synthesised by using a nano-porous Ni-template via a chemical vapor deposition (CVD) method, as described in detail elsewhere [45–49]. In short, the CVD process was performed at 800 °C for 5 min for graphene growth. The as-grown NPG acquired the 3D morphology of the Ni substrate, and then it was exfoliated by chemical etching of the substrate by 1.0 M HCl solution. The resulting NPG sample sized 1–2 cm^2 with ~30 μm thickness was obtained. Transmission electron microscopy images and diffraction patterns, reported elsewhere [39], reveal moiré superstructures, indicating the coexistence of single-layer and turbostratic bi-layer graphene in the pristine NPG samples.

Deuteration has been performed in-situ in ultra-high vacuum (UHV) by exposing NPG to atomic D, which is produced by D_2 cracking into a capillary source locally heated at 2100 °C. Compared to previous works [41,50], we used here longer exposure times, beyond the XPS saturation signal, and low-energy (~0.175 eV) neutral deuterium atoms rather than low-energy ions. Remarkably, the deuterium atoms penetrate more deeply into the porous structure of NPG, giving rise to the intense Raman D band visible in Fig. 1(b).

2.2. Sample characterization

The integrated XPS/micro-Raman and UPS measurements[1] were carried out in UHV chambers, with a base pressure in the low 10^{-10} mbar range. Core-level photoelectrons were excited by a X-ray Mg K_α (1253.6 eV) photon source, and analyzed by a hemispherical electron analyzer VG Microtech Clam-2 in constant pass energy (PE) mode set at 50 eV, with energy resolution better than 1.0 eV. The binding energy (BE) scale was calibrated on a freshly sputtered gold foil in electrical contact with the sample, by acquiring the Au $4f_{7/2}$ core-level set at 84.0 eV after each measurement. The UPS data have been taken with a Gammadata VUV 5000 microwave excited monochromatised He source, with He-I_α radiation (21.218 eV). Photoelectrons were analyzed with an electrostatic hemisferical Scienta SES 200 analyzer equipped with a multi-channel-plate detector, operated with an overall 20 meV energy resolution. Raman experiments were excited by a single frequency Nd:YVO_4 laser at 532 nm. Measurements were acquired in a backscattering configuration, using a vacuum-compatible 60× objective (NA = 0.82). The laser power was kept below 250 mW to avoid sample damage. A 0.5 m focal length monochromator, equipped with a 1200 or 300 grooves/mm grating, was employed to spectrally analyse the Raman signal, which was detected by a back-illuminated liquid nitrogen-cooled Si CCD Camera. The reflected laser light was filtered out by a super-notch filter. The sample was mounted on a x-y-z piezoelectric stage for performing Raman maps.

2.3. HREELS measurements

HREEL measurements[2] were taken on pristine and deuterated samples, in both the [0–4000 cm^{-1}] vibrational and the [0–6] eV electronic ranges. Measurements were taken with primary energy $E_p = 9.0$ eV, and angle of incidence $\theta_i = 52^\circ$. The elastic peak intensity was rather small (few tens of kcps) and strongly decreased with primary energy, hindering measurements for E_p greater than 12 eV. Moreover, it showed no dependence on both the incidence and the collection angles. This latter finding is related to the ill-defined orientation of the sample surface, making the dipolar lobe extremely broad. This in turn means that impact-scattering events contribute significantly to the spectra and that indirect excitations (i.e., with $q \neq 0$) should be taken into account in analyzing the spectra. Moreover, it also means that dipole selection rules do not strictly apply in this case, allowing us to observe all infra-red (IR) active modes, with dipole both parallel and normal to the surface.

2.4. Theoretical modelling

In order to complement the above detailed XPS, UPS and HREELS measurements, we carried out a first-principles investigation of a series of hydrogenated single-layer and bi-layer graphene structures, which are known to cohexist in the pristine NPG samples, as mentioned above and fully detailed elsewhere [26,39]. For the single-layer structures, we studied both single-side H/D graphene (1-side H/D-Gr or graphone [51–53], corresponding to 50% hydrogenation of the C sites) and two-side H/D graphene (2-side H/D-Gr or graphane [10,28,54]). For this, the boat conformer [55] of graphone (Fig. 2(b), top left panel) and the chair conformer of graphane [28] (Fig. 2(b), top right panel) were considered, being the most stable structures.[3] For the hydrogenated bi-layer structures (2-side H/D-2LGr, also referred to as diamanes [57]), we consid-

[1] The integrated XPS/micro-Raman measurements were carried out at the SmartLab and the UPS at the LOTUS laboratory of the Department of Physics at Sapienza University of Rome.

[2] The HREELS experiments were performed at Modena and Reggio Emilia University in Modena, in the SESAMO laboratory.

[3] The chair conformer of graphone, known to exhibit a ferromagnetic phase, was not considered here due to its poor stability in the absence of a support surface [52,56].

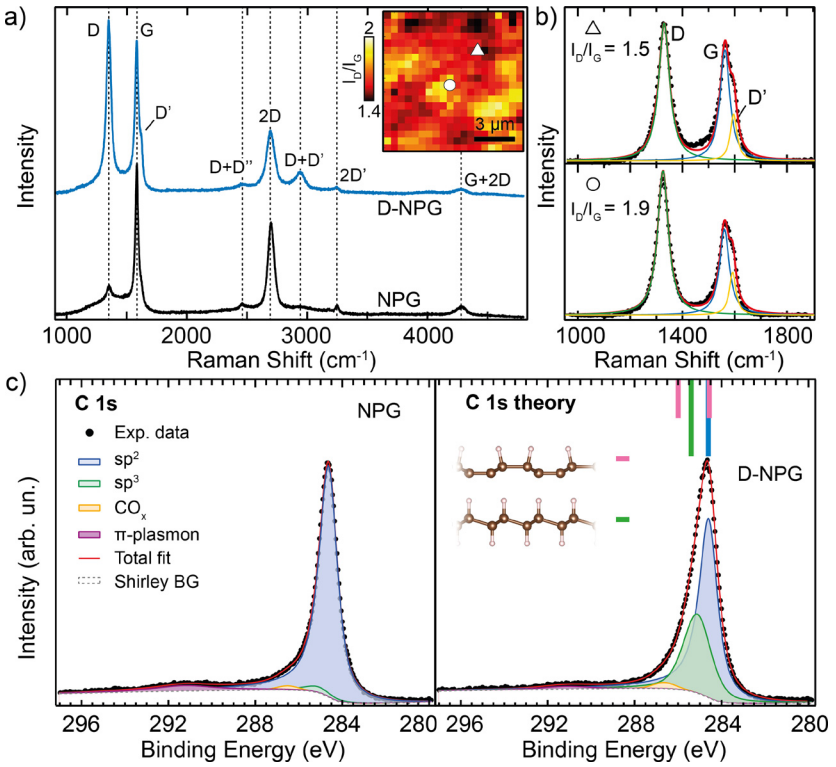

Fig. 1. (a) Micro-Raman spectra for UHV-clean NPG (black curve) and after 300 min of atomic D exposure (D-NPG, blue curve). Inset: spatial dependence of the ratio of the D and G peaks intensities elaborated from a micro-Raman map of a 10×10 μm^2 region of the D-NPG sample scanned in steps of 500 nm. (b) Two micro-Raman spectra displaying the D and G peaks energy region recorded at the points highlighted in the map of panel a) (triangle and circle, respectively), and fitted to three Lorentzian peaks. (c) C 1s core level XPS spectra of UHV-clean NPG (left) and D-NPG (right). Experimental data (dots), sp^2 (blue peaks) and sp^3 (green peaks) fitting components, CO_x component (yellow peak), π plasmon (violet peak), total fit (red line), and Shirley background (white) are displayed; in the inset to the right panel, simulated core-level binding energies for the H–C configurations depicted in the inset are indicated by vertical bars, as referenced to pristine Gr (blue bar). (For interpretation of the references to colour in this figure legend, the reader is referred to the web version of this article.)

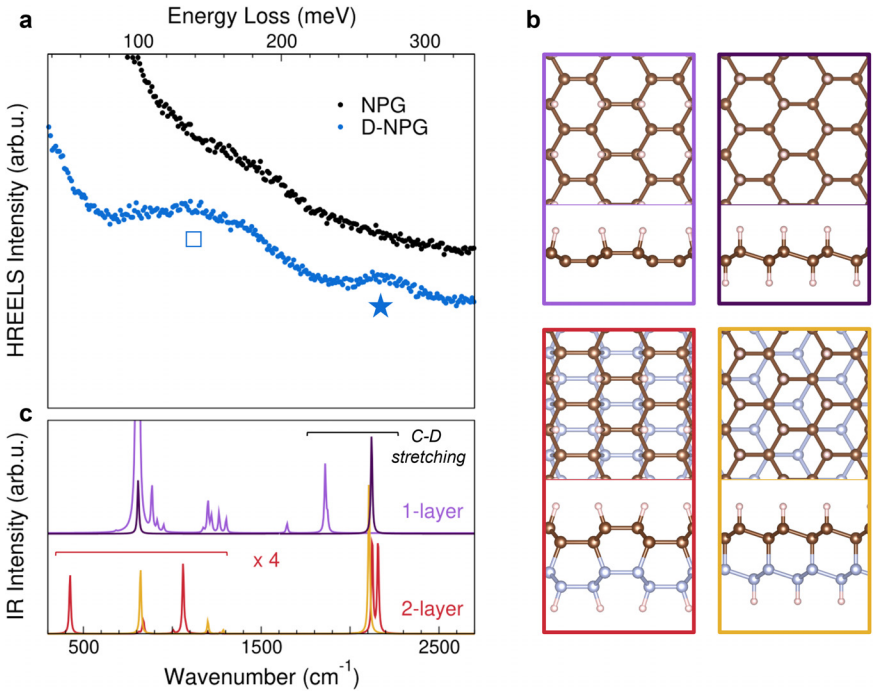

Fig. 2. (a) HREEL vibrational spectra of NPG (black dots) and D-NPG (blue dots). The NPG spectrum has been upshifted for clarity (complete, unshifted spectra are reported in Supplementary material). (b) Ball-and-stick models (top and side views) of 1-side (light violet, top left) and 2-side (dark violet, top right) single-layer D-Gr, as well as boat (red, bottom left) and chair (orange, bottom right) conformers of 2-side bilayer D-Gr. (c) Simulated IR spectra for the structures in (b), displayed with the same colour code. The energy range displayed on the x axis is the same as in panel (a), but in different units. (For interpretation of the references to colour in this figure legend, the reader is referred to the web version of this article.)

ered both AA- and AB-stacking of the chair conformer [58,59] (the latter shown in Fig. 2(b), bottom left panel), as well as the boat conformer [58] (Fig. 2(b), bottom right panel). These structures have been shown to form diamond-like lattice structures by binding two graphene layers together in the presence of adsorbed hydrogen, thus forming interlayer C–C bonds that can stabilise a turbostratic stacking arrangement [59].

The ground-state properties of the hydrogenated (deuterated) graphene structures described above were obtained from ab-initio DFT simulations, as implemented in the QUANTUM ESPRESSO software package [60–62]. In particular, core-level shifts (CLS) for different percentages of H adsorbed on a Gr layer were computed for the optimized structures by resorting to the so-called core-hole Delta Kohn-Sham (Δ-KS) approach [63], which demonstrated successful in reproducing experimental CLS for graphene-based systems [64]; phonon frequencies and IR intensities were calculated within the framework of density-functional perturbation theory (DFPT) [65], following the same approach previously used for nanosized graphenes [66]. Further details on the used methodologies are reported in Supplementary material.

Dielectric properties were computed for the above structures by including of electron-electron (e-e) and electron-hole (e-h) interactions

within an ab-initio many-body perturbation theory (MBPT) approach, as implemented in the YAMBO code [67,68]. Quasiparticle band structures (together with density of states) were obtained within the *GW* approximation in the non-self-consistent G_0W_0 scheme [69]; EEL spectra were obtained from the imaginary part of the macroscopic dielectric function, resulting from the solution of the BSE [69], by taking into account that absorption and loss spectra coincide in the long-wavelength limit for low-dimensional systems [70]. For these calculations, which require the control over a large set of (interdependent) parameters to obtain reliable results, converged parameters were obtained by employing an automated AIIDA-YAMBO based workflow [71]. These computational data, including atomic structures, input, and output files, are available on Materials Cloud,[4] whereas further details on the approximations employed are reported in Supplementary material.

3. Results and discussion

The Raman spectra of NPG, in clean pristine form and after exposure to atomic deuterium, are shown in Fig. 1(a,b). The Raman spectrum of pristine NPG (black line, panel a) is dominated by G (1583 cm^{-1}) and 2D (2700 cm^{-1}) bands, which are associated to the in-plane sp^2 graphene lattice [72].[5] The presence of very small D (1350 cm^{-1}) and D′ (1618 cm^{-1}) peaks is a marker of high-quality samples, indicating the absence of lattice distortions of the pristine graphene mesh [72]. Upon deuteration (blue line spectrum in Fig. 1(a)), a strong increase of the D peak intensity is observed, along with a slight increase of both D' and D + D′ bands, which can be associated to the sp^3 bond formation typical of hydrogenated Gr [10]. The homogeneity of the deuteration process is evaluated by spatially resolved micro-Raman measurements. The inset to Fig. 1(b) shows a micro-Raman map of the I_D/I_G intensity ratio extracted from a 10×10 μm^2 region of the D-NPG sample. A Lorentzian fitting analysis of the relevant Raman bands (two examples of which are shown in Fig. 1(b), corresponding to the two points marked in the inset of panel a) shows an I_D/I_G distribution centered at 1.7 with a 0.3 spread, suggesting a rather homogeneous deuterium uptake. It is worth noting that a depth profile micro-Raman analysis focused down to about 1 μm below the surface displayed an analogous homogeneous distribution [73], thus suggesting an effective deuteration deep into the NPG pores.

To better quantify the atomic deuterium uptake, we resort to surface-sensitive C 1s core-level photoemission spectroscopy. Figure 1(c) shows the C 1s core level spectra acquired at the clean and deuterated NPG samples, as compared to the DFT predictions for different H-Gr configurations (vertical lines). For clean pristine NPG, the C 1s core level spectrum presents a dominant peak at 284.6 eV BE, which is associated to the semimetallic graphene signal with a planar sp^2 hybridization, in agreement with previous results [39,40]. The presence of a tiny sp^3 component at 285.2 eV is associated to the distortion of the planar Gr structure due to the tubular wrinkled portion of NPG [39,40].

In the deuterated sample, atomic deuterium uptake is revealed by the presence of an increased sp^3 component with respect to the pristine planar C–C sp^2 configuration, as can be deduced by the C 1s core level fitting,[6] where the distortion of the sp^2 configuration towards an sp^3 hybridization is due to the chemisorption of D adatoms on top of the C sites [26,28]. At the same time, we observe an intensity reduction of the intrinsic plasmon associated to the π collective excitations at about 291.1 eV after deuteration, which can be attributed to the frustrated collective π plasmon modes associated with the conversion from the pristine semimetallic to a semiconducting phase [41]. The deuteration process is very clean, as only a very tiny component due to residual CO_x bonds (< 2%) is observed at about 286.5 eV BE. Moreover, the measured C 1s spectra do not unveil any contributions at lower BE with respect to the sp^2 peak due to unsaturated C dangling bonds at vacancy sites [74], both before and after deuteration. This indicates that the D chemisorption process is not inducing any damage in the NPG crystal lattice.

The increased intensity in the sp^3 component with respect to the sp^2 one allows the evaluation of the fraction of D atoms bound to C atoms in the NPG mesh. By considering the relative intensity ratio $\Theta = I(sp^3)/[I(sp^2) + I(sp^3)]$, the Θ value increases from less than 4 at. % on the pristine NPG to about 36 at. % for D-NPG. The persistence of a sp^2 component in the D-NPG sample is due to the presence of only a fraction of deuterium atoms in four-fold coordination with the C atoms in the graphene mesh, consistent with the permanence of the Raman G and 2D bands, which should be quenched upon deuterium adsorption due to in-plane sp^2 translation symmetry breaking.

CLS predictions with respect to pristine Gr were obtained from DFT simulations by considering different % of H adsorbed on a Gr layer (see Supplementary material). The corresponding BEs, obtained by taking the experimental pristine Gr component as a reference (284.6 eV, blue bar), are depicted as vertical bars above the C 1s data of the deuterated sample (right panel of Fig. 1(c)) for 50 and 100% H–C configurations (see inset; configurations are labelled according to the bar colour code). The bar height indicates the relative weight of each component for a given H–C configuration. We find that the 50% single-side H–C configuration presents two inequivalent C atoms, giving rise to two CL shifted components (pink bars), at −0.1 eV (i.e. 284.5 eV BE) and 1.3 eV (i.e. 285.9 eV BE), associated to sp^2 three-fold and sp^3 four-fold C coordination, respectively. The 100% 2-side H–C configuration (green bar) presents a single sp^3 component at 285.4 eV (0.8 eV CLS), in much better agreement with the C 1s experimental value for the sp^3 component (285.2 eV), as deduced by the fitting procedure.

More detailed information on the deuterium adsorption configuration can be obtained by HREELS, a vibrational electron scattering spectroscopy technique very sensitive to IR-active modes. HREEL vibrational spectra of pristine (black dots) and deuterated (blue dots) NPG samples are shown in Fig. 2(a), where we focus on the [300–2700] cm^{-1} (37–335 meV) frequency range (see Supplementary material for further details on the full spectral range). The clean NPG spectrum is mainly dominated by a Drude tail characteristic of semimetallic graphene, which underlies a faint structure located at about 1450 cm^{-1} (~180 meV), attributed to both graphene-like optical (C–C stretching) modes [75] and C–H bending modes arising from residual H present on the sample after annealing (see Figure and related discussion in Supplementary material).

The spectrum of D-NPG displays instead two main features, one extending across the [900–1500] cm^{-1} (112–186 meV) range and one at about 2180 cm^{-1} (270 meV), indicated with □ and ★, respectively. The latter (★) – not present in the pristine sample – represents the clear signature of NPG deuteration, and can be unequivocally attributed to C–D stretching modes, which typically lie in the [1900-2200] cm^{-1} range [76–82]. As discussed in detail below, its exact frequency value depends on the specific configuration of D adsorption, and thus provides valuable information on the structural details of the deuterated sample. As far as the former (□) is concerned, it can originate from both C–D/C–H bending modes [83] and graphene-like optical modes, given its partial overlap with the feature at about 1450 cm^{-1} (180 meV) of the clean pristine sample.

In order to complement the above HREEL analysis, we carried out a detailed vibrational study based on DFT, which provides an atomistic comprehension of the specific deuterium adsorption configurations. Figure 2(c) shows the IR-active modes computed for the structures depicted in panel b and described above (see Materials and methods Section). Peaks appearing in the [1800–2200] cm^{-1} region can be attributed to C–D stretching modes. In particular, while 1-side deuteration (light violet curve) gives rise to a peak at about 1860 cm^{-1}, the

[4] See https://doi.org/10.24435/materialscloud:9b-34

[5] The G and 2D bands correspond, respectively, to the symmetry-allowed E_{2g} phonon at the Brillouin zone center Γ, and to an in-plane breathing of the hexagonal rings at the *K* point associated with a double resonance process.

[6] Details on the fitting procedure are described in Ref. [50]

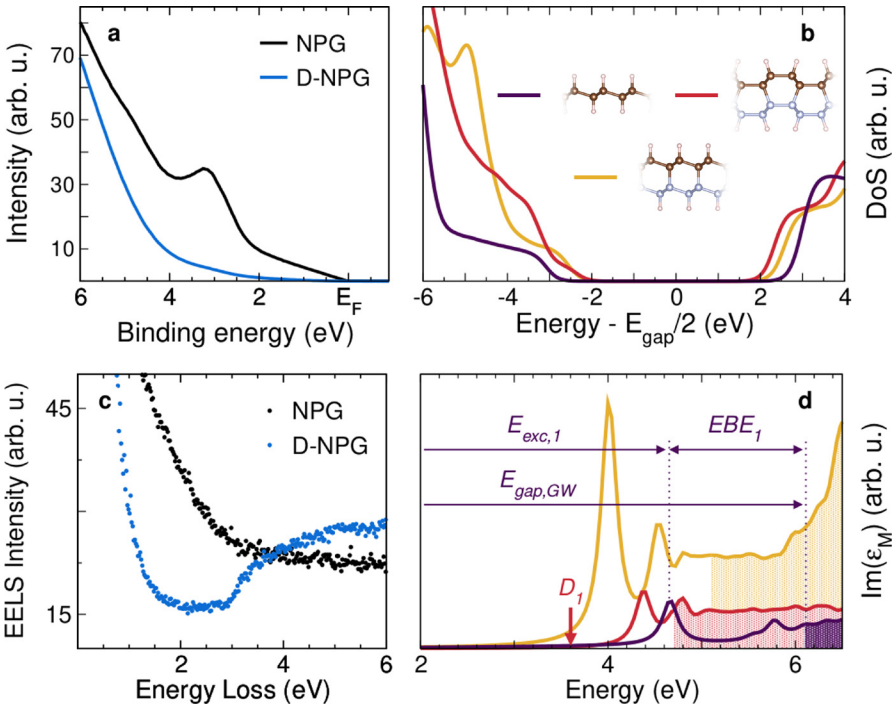

Fig. 3. (a) Experimental VB spectra for clean NPG (black) and deuterated NPG (blue). (b) Simulated G_0W_0 density of states (DoS) for the models in the inset (see also Fig. 2(b)); zero energy set at midgap; a homogenous broadening of 140 meV is applied. (c) HREEL spectra of pristine NPG (black) and deuterated NPG (blue). (d) Calculated Im(ϵ_M) in the optical limit ($q \to 0$), for the models in the inset of panel b. The binding energy of the n^{th} exciton (EBE_n) can be read as the difference between the GW gap $E_{gap,GW}$ and the corresponding excitation energy $E_{exc,n}$, here exemplified for the first exciton of the 2-side H-Gr (violet curve). A Lorentzian broadening of 0.1 eV has been included. The continuum region is indicated as coloured shaded area. (For interpretation of the references to colour in this figure legend, the reader is referred to the web version of this article.)

modes of the 2-side deuterated structures lie at 2100–2160 cm^{-1} (dark violet, red and orange curves), irrespective of the specific conformer (sigle- or bi-layer, with different registry). Our results are comparable to those obtained for hydrogenated graphene in Refs. [77,84–87], where a similar result for 1-side and 2-side hydrogenation is presented. A comparison with the experimentally observed C–D stretching frequency described above clearly shows that only the 2-side deuterated models are consistent with experimental data, while 1-side deuteration can be ruled out. At lower wavenumbers (500–1500 cm^{-1} range), several peaks are predicted for both 1- and 2-side configurations, and assigned to C–D bending modes from inspection of the atomic displacements. Looking at the experimental broad feature in this frequency range (□), one envisages a significant contribution coming from these C–D bending modes, even though the broadness of the experimental feature and the possible contribution from other modes at similar frequencies (e.g. C–C and C–H, see discussion above) hinders a more detailed comparison between experimental and theoretical features in this frequency range.

The picture discussed so far for deuterium adsorption on graphene, as obtained by the vibrational experimental and theoretical analysis, ensures the formation of stable D–C bonds on both sides of the graphene sheet, thus leading to the conversion of free-standing, unsupported graphene into a stable prototype of graphane, characterised by the opening of an energy gap [26,41,50]. The electronic structure and dielectric response of NPG and D-NPG in the eV energy range, as studied by photoemission and HREELS, is displayed in Fig. 3, where we show the evolution of the electronic properties and dielectric response from the pristine NPG (black, panels a,c) to its deuterated phase (blue). The integrated intensity of the photoemitted electrons from the valence band (VB) of NPG (Fig. 3(a)) presents a linear spectral density close to the Fermi level E_F, due to the electronic state dispersion close to the apex of the Dirac cone, and a peak at ~3.2 eV related to a maximum of the density of 2p-π states. After deuteration (blue line, Fig. 3(a)), the linear spectral density below E_F and of the 2p-π peak – both signatures of a graphene phase – are noticeably reduced. Moreover, the VB maximum shifts to ~3.5 eV, suggesting a large gap opening, in agreement with previous findings for highly hydrogenated NPG [26], clearly denoting the transition to a semiconducting phase. The presence of a faint tail in the low-BE (blue line) can be attributed to the residual spectral density of pristine NPG due to the partial deuteration of the sample (see previous discussion on the intensity ratio of C 1s components).

The dielectric response and gap opening of deuterated NPG is further investigated by HREELS measurements, as displayed in Fig. 3(c). Whereas the clean NPG spectrum (black dots) solely displays a broad Drude-like tail, due to its semimetallic character, the deuterated phase shows a substantial decrease of the Drude-like tail intensity in the region between 0 and ~3 eV energy loss, accompanied by the appearance of a transition onset located at 3.25 ± 0.1 eV (see Supplementary material for details on the edge-evaluation procedure). These spectral features clearly demonstrate the opening of a semiconducting gap upon deuteration. The observed onset is in fair agreement with the optical gap of about 4 eV reported for chemichally derived H-Gr [25], especially considering the contribution of finite-momentum excitations to our EEL spectra (see discussion below). Other previous reports on dielectric and optical properties of H-Gr are either strongly affected by substrate effects [12], or mostly dominated by lower energy broad emission arising from unsaturated nano-graphene domains [29,88]. We note that the presence of smaller sp^2-C clusters may in principle be responsible for absorption features at these energies, which are however accompanied by prominent features at low BE in the VB spectrum [23]. In our case, the VB spectrum in Fig. 3(a) rules out the presence of any of those features, thus allowing us to safely disregard their possible contribution also to the EEL spectrum. The observed semiconducting gap opening at 3.25 eV can be therefore attributed to the intrinsic properties of H-Gr.

Further insight into the fundamental and optical gap of free-standing H-Gr, as probed here by photoemission and HREEL spectroscopies, respectively, can be obtained from ab-initio simulations by including e-e and e-h interactions. Figure 3(b) shows the fundamental gap in the G_0W_0 approximation for all the double-side hydrogenated systems previously discussed in Fig. 2(b). We neglect the single-side hydrogenation, which was ruled out according to the vibration analysis (see above). Depending on the specific configuration, the gap $E_{gap,GW}$ ranges between 4.7 and 6.1 eV, with a VB maximum located at $-E_{gap,GW}/2$ (i.e. −2.35 and −3.05 eV respectively) if we consider E_F lying at mid-gap in the absence of doping, as previously discussed in Ref. [26]. Taking into

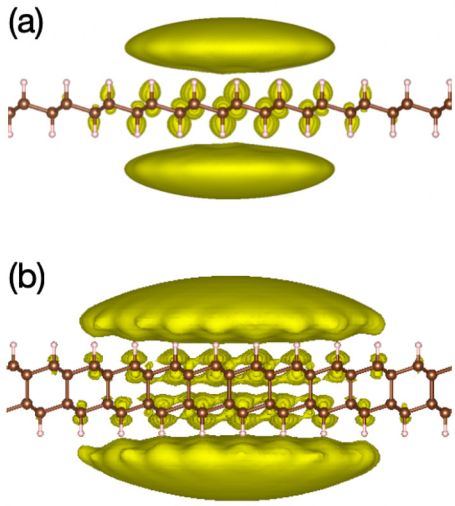

Fig. 4. Electron probability distribution for the lowest excitons in single- (a) and bi-layer (b) H-Gr configurations. The hole is fixed on a C–C bond.

account that experimental NPG samples are constituted by single and bi-layer graphene (in turbostratic arrangement), the calculated range of *GW* VB maximum values compares well with the experimental value of 3.5 eV.

Figure 3 (d) shows the calculated optical absorption spectra for the same configurations, which is characterized by a step-like shape (shaded area), typical of 2D semiconductors, with prominent individual excitonic peaks lying below the onset of the continuum (shaded area). The optical gap ranges from 4 (orange curve) to 4.66 eV (violet curve), to be compared with the experimental onset of about 3.25 eV. The discrepancy is likely related to the fact that we are here considering the optical response of ideal systems in vacuum with perfect registry. The real material comprises instead single- and few-layer regions with misoriented (turbostratic) stacking – all averaged in a macroscopic EELS measurement –, which can give rise to quantitatively different excitations, including optically inactive ones (see below) that may become relevant when probing the sample at finite momentum.

The exciton binding energy (*EBE*) of the lowest lying excitation with respect to the continuum is predicted to exceed 1 eV, irrespective of the specific free-standing configuration computed here, as can be seen in Fig. 3(d) by comparing the excitation energy of the first exciton, $E_{exc,1}$ with the *GW* gap (exemplified in panel f for 2-side H-Gr, violet curve, where the EBE_1 amounts to 1.44 eV). This holds true also for the boat conformer of 2-side H-2LGr (red curve), for which the first bright exciton corresponds to the 19th excitation, while the first excitation lies at about 3.6 eV, with EBE_1 = 1.1 eV. Such a large value results from both the enhanced e-h interaction in reduced dimensions and the weak screening of few-atom-thick free-standing systems in vacuum, as previously found for other low-dimensional materials [89,90].

To better understand the nature of the excitations and their dependence on the different conformers, we analyse the excitonic wavefunctions, which are inspected by fixing the hole position in the centre of the C–C bond, where the valence states are located, and by plotting the electron probability density (see Fig. 4). For both single- (a) and bilayer H-Gr (b), we find that the lowest lying excitons have a charge transfer character, with the hole localized on the C–C bond and the electron having mixed C–H localization and free-electron-like character, as shown by Cudazzo et al. [18] for single-layer graphane. This again demonstrates that the optical properties of the system are robust irrespective of the actual configuration considered (e.g. single- or bilayer).

4. Conclusions

Well-defined hallmarks of the conversion of semimetallic graphene into a semiconducting phase through hydrogen incorporation have been identified thanks to a joint core-level and electron-energy loss spectroscopy study, in conformity with theoretical predictions. Atomic deuterium chemisorption on fully free-standing and unsupported graphene, by using NPG and low-energy molecular cracking in UHV, induces the formation of sp^3 hybridized chemical bonds, as determined by photoemission spectroscopy. Thanks to the use of a hydrogen isotope and with the support of ab-initio calculations, characteristic D–C stretching frequencies are monitored in the HREEL vibrational spectrum, allowing for unequivocally identifying the adsorption configuration on both sides of the NPG veils. These signatures prefigure a semiconducting phase, confirmed by a wide optical band gap opening and by the presence of enhanced e–h interactions with respect to the pristine semimetallic phase, which is crucial for both fundamental knowledge of 2D materials and for emerging applications of graphene in electronic and opto-electronic devices.

CRediT authorship contribution statement

Maria Grazia Betti: Conceptualization, Supervision, Writing - original draft. **Dario Marchiani:** Investigation, Formal Analysis, Visualization. **Andrea Tonelli:** Investigation, Formal analysis. **Marco Sbroscia:** Investigation. **Elena Blundo:** Investigation, Formal Analysis. **Marta De Luca:** Investigation, Formal Analysis. **Antonio Polimeni:** Investigation. **Riccardo Frisenda:** Investigation, Formal Analysis, Visualization. **Carlo Mariani:** Conceptualization, Funding acquisition, Writing - original draft. **Samuel Jeong:** Resources. **Yoshikazu Ito:** Funding acquisition, Resources. **Nicola Cavani:** Investigation. **Roberto Biagi:** Investigation. **Peter N. O. Gillespie:** Investigation, Formal Analysis. **Michael A. Hernandez Bertran:** Investigation, Formal Analysis. **Miki Bonacci:** Investigation, Formal Analysis and Data Curation. **Elisa Molinari:** Supervision, Funding acquisition. **Valentina De Renzi:** Supervision, Writing - original Draft. **Deborah Prezzi:** Conceptualization, Supervision, Investigation, Visualization, Writing - original draft. All authors discussed the results and commented on the manuscript at all stages.

Declaration of Competing Interest

The authors declare that they have no known competing financial interests or personal relationships that could have appeared to influence the work reported in this paper.

Data availability

Data will be made available on request.

Acknowledgements

This work was partially supported by: Centre of Excellence MaX – Materials design at the eXascale, funded by the European Union programs H2020-INFRAEDI-2018-1 (Grant no. 824143) and HORIZON-EUROHPC-JU-2021-COE-1 (Grant no. 101093374); SUPER (Supercomputing Unified Platform-Emilia-Romagna) regional project; JSPS KAKENHI program (Grant no. JP21H02037); PRIN-MIUR FERMAT project (Grant no. 2017KFY7XF);“La Sapienza” Ateneo funds. Computer time on the Marconi100 machine at CINECA was provided by the Italian ISCRA program.

Supplementary material

Supplementary material associated with this article can be found, in the online version, at doi:10.1016/j.cartre.2023.100274.

References

[1] J. Liu, J. Tang, J.J. Gooding, Strategies for chemical modification of graphene and applications of chemically modified graphene, J. Mater. Chem. 22 (2012) 12435–12452.

[2] K.E. Whitener, Review article: hydrogenated graphene: a user's guide, J. Vac. Sci. Technol. A 36 (5) (2018) 05G401.

[3] Y. Fei, S. Fang, Y.H. Hu, Synthesis, properties and potential applications of hydrogenated graphene, Chem. Eng. J. 397 (2020) 125408.

[4] V. Tozzini, V. Pellegrini, Prospects for hydrogen storage in graphene, Phys. Chem. Chem. Phys. 15 (2013) 80–89.

[5] I.A. Baburin, A. Klechikov, G. Mercier, A. Talyzin, G. Seifert, Hydrogen adsorption by perforated graphene, Int. J. Hydrog. Energy 40 (20) (2015) 6594–6599.

[6] R. Nagar, B.P. Vinayan, S.S. Samantaray, S. Ramaprabhu, Recent advances in hydrogen storage using catalytically and chemically modified graphene nanocomposites, J. Mater. Chem. A 5 (2017) 22897–22912.

[7] J.R. Morse, D.A. Zugell, E. Patterson, J.W. Baldwin, H.D. Willauer, Hydrogenated graphene: important material properties regarding its application for hydrogen storage, J. Power Sources 494 (2021) 229734.

[8] X. Han, X. Tong, X. Liu, A. Chen, X. Wen, N. Yang, X.-Y. Guo, Hydrogen evolution reaction on hybrid catalysts of vertical MoS_2 nanosheets and hydrogenated graphene, ACS Catal. 8 (3) (2018) 1828–1836.

[9] A.H. Reshak, Chairlike and boatlike graphane: active photocatalytic water splitting solar-to-hydrogen energy conversion under UV irradiation, J. Phys. Chem. C 122 (15) (2018) 8076–8081.

[10] D.C. Elias, R.R. Nair, T.M.G. Mohiuddin, S.V. Morozov, P. Blake, M.P. Halsall, A.C. Ferrari, D.W. Boukhvalov, M.I. Katsnelson, A.K. Geim, K.S. Novoselov, Science 323 (2009) 610–613.

[11] P. Gowda, D.R. Mohapatra, A. Misra, Enhanced photoresponse in monolayer hydrogenated graphene photodetector, ACS Appl. Mater. Interfaces 6 (19) (2014) 16763–16768.

[12] J. Son, S. Lee, S.J. Kim, B.C. Park, H.-K. Lee, S. Kim, J.H. Kim, B.H. Hong, J. Hong, Hydrogenated monolayer graphene with reversible and tunable wide band gap and its field-effect transistor, Nat. Commun. 7 (1) (2016) 13261.

[13] S. Li, J. Li, Y. Wang, C. Yu, Y. Li, W. Duan, Y. Wang, J. Zhang, Large transport gap modulation in graphene via electric-field-controlled reversible hydrogenation, Nat. Electron. 4 (2021) 254–260.

[14] S. Li, C. Yu, Y. Wang, K. Zhang, K. Jiang, Y. Wang, J. Zhang, Tafel-kinetics-controlled high-speed switching in a electrochemical graphene field-effect transistor, ACS Appl. Mater. Interfaces 14 (42) (2022) 47991–47998.

[15] S.M. Tan, Z. Sofer, M. Pumera, Biomarkers detection on hydrogenated graphene surfaces: towards applications of graphane in biosensing, Electroanalysis 25 (3) (2013) 703–705.

[16] A.N. Banerjee, Graphene and its derivatives as biomedical materials: future prospects and challenges, Interface Focus 8 (3) (2018) 20170056.

[17] M. Chakik, S. Bebe, R. Prakash, Hydrogenated graphene based organic thin film transistor sensor for detection of chloride ions as corrosion precursors, Appl. Sci. 12 (2) (2022).

[18] P. Cudazzo, C. Attaccalite, I.V. Tokatly, A. Rubio, Strong charge-transfer excitonic effects and the Bose–Einstein exciton condensate in graphane, Phys. Rev. Lett. 104 (2010) 226804.

[19] Z. Jiang, W. Lou, Y. Liu, Y. Li, H. Song, K. Chang, W. Duan, S. Zhang, Spin-triplet excitonic insulator: the case of semihydrogenated graphene, Phys. Rev. Lett. 124 (2020) 166401.

[20] H. Katow, R. Akashi, Y. Miyamoto, S. Tsuneyuki, First-principles study of the optical dipole trap for two-dimensional excitons in graphane, Phys. Rev. Lett. 129 (2022) 047401.

[21] S. Lebègue, M. Klintenberg, O. Eriksson, M.I. Katsnelson, Accurate electronic band gap of pure and functionalized graphane from GW calculations, Phys. Rev. B 79 (2009) 245117.

[22] P. Cudazzo, L. Sponza, C. Giorgetti, L. Reining, F. Sottile, M. Gatti, Exciton band structure in two-dimensional materials, Phys. Rev. Lett. 116 (2016) 066803.

[23] Z. Luo, J. Shang, S. Lim, D. Li, Q. Xiong, Z. Shen, J. Lin, T. Yu, Modulating the electronic structures of graphene by controllable hydrogenation, Appl. Phys. Lett. 97 (23) (2010) 233111.

[24] B.R. Matis, J.S. Burgess, F.A. Bulat, A.L. Friedman, B.H. Houston, J.W. Baldwin, Surface doping and band gap tunability in hydrogenated graphene, ACS Nano 6 (1) (2012) 17–22.

[25] Y. Yang, Y. Li, Z. Huang, X. Huang, $(C_{1.04}H)_n$: a nearly perfect pure graphane, Carbon 107 (2016) 154–161.

[26] M.G. Betti, E. Placidi, C. Izzo, E. Blundo, A. Polimeni, M. Sbroscia, J. Avila, P. Dudin, K. Hu, Y. Ito, D. Prezzi, M. Bonacci, E. Molinari, C. Mariani, Gap opening in double-sided highly hydrogenated free-standing graphene, Nano Lett. 22 (7) (2022) 2971–2977.

[27] M.H.F. Sluiter, Y. Kawazoe, Cluster expansion method for adsorption: application to hydrogen chemisorption on graphene, Phys. Rev. B 68 (2003) 085410.

[28] J.O. Sofo, A.S. Chaudhari, G.D. Barber, Graphane: a two-dimensional hydrocarbon, Phys. Rev. B 75 (2007) 153401.

[29] R.A. Schäfer, J.M. Englert, P. Wehrfritz, W. Bauer, F. Hauke, T. Seyller, A. Hirsch, On the way to graphane-pronounced fluorescence of polyhydrogenated graphene, Angew. Chem. Int. Ed. 52 (2) (2013) 754–757.

[30] V. Strauss, R.A. Schäfer, F. Hauke, A. Hirsch, D.M. Guldi, Polyhydrogenated graphene: excited state dynamics in photo- and electroactive two-dimensional domains, J. Am. Chem. Soc. 137 (40) (2015) 13079–13086.

[31] R.A. Schäfer, D. Dasler, U. Mundloch, F. Hauke, A. Hirsch, Basic insights into tunable graphene hydrogenation, J. Am. Chem. Soc. 138 (5) (2016) 1647–1652.

[32] Z. Luo, T. Yu, K.-j. Kim, Z. Ni, Y. You, S. Lim, Z. Shen, S. Wang, J. Lin, Thickness-dependent reversible hydrogenation of graphene layers, ACS Nano 3 (7) (2009) 1781–1788.

[33] S. Ryu, M.Y. Han, J. Maultzsch, T.F. Heinz, P. Kim, M.L. Steigerwald, L.E. Brus, Reversible basal plane hydrogenation of graphene, Nano Lett. 8 (12) (2008) 4597–4602.

[34] K.E. Whitener, W.K. Lee, P.M. Campbell, J.T. Robinson, P.E. Sheehan, Chemical hydrogenation of single-layer graphene enables completely reversible removal of electrical conductivity, Carbon 72 (2014) 348–353.

[35] R. Balog, M. Andersen, B. Jørgensen, Z. Sljivancanin, B. Hammer, A. Baraldi, R. Larciprete, P. Hofmann, L. Hornekær, S. Lizzit, Controlling hydrogenation of graphene on Ir(111), ACS Nano 7 (5) (2013) 3823–3832.

[36] S. Rajasekaran, F. Abild-Pedersen, H. Ogasawara, A. Nilsson, S. Kaya, Interlayer carbon bond formation induced by hydrogen adsorption in few-layer supported graphene, Phys. Rev. Lett. 111 (2013) 085503.

[37] D. Lizzit, M.I. Trioni, L. Bignardi, P. Lacovig, S. Lizzit, R. Martinazzo, R. Larciprete, Dual-route hydrogenation of the graphene/Ni interface, ACS Nano 13 (2) (2019) 1828–1838.

[38] C. Lee, N. Leconte, J. Kim, D. Cho, I.-W. Lyo, E. Choi, Optical spectroscopy study on the effect of hydrogen adsorption on graphene, Carbon 103 (2016) 109–114.

[39] I. Di Bernardo, G. Avvisati, C. Mariani, N. Motta, C. Chen, J. Avila, M.C. Asensio, S. Lupi, Y. Ito, M. Chen, T. Fujita, M.G. Betti, Two-dimensional hallmark of highly interconnected three-dimensional nanoporous graphene, ACS Omega 2 (7) (2017) 3691–3697.

[40] I. Di Bernardo, G. Avvisati, C. Chen, J. Avila, M.C. Asensio, K. Hu, Y. Ito, P. Hines, J. Lipton-Duffin, L. Rintoul, N. Motta, C. Mariani, M.G. Betti, Topology and doping effects in three-dimensional nanoporous graphene, Carbon 131 (2018) 258–265.

[41] M.M.S. Abdelnabi, E. Blundo, M.G. Betti, G. Cavoto, E. Placidi, A. Polimeni, A. Ruocco, K. Hu, Y. Ito, C. Mariani, Towards free-standing graphane: atomic hydrogen and deuterium bonding to nano-porous graphene, Nanotechnology 32 (3) (2020) 035707.

[42] M.G. Betti, M. Biasotti, A. Boscá, F. Calle, J. Carabe-Lopez, G. Cavoto, C. Chang, W. Chung, A. Cocco, A. Colijn, J. Conrad, N. D'Ambrosio, P. de Salas, M. Faverzani, A. Ferella, E. Ferri, P. Garcia-Abia, G.G. Gomez-Tejedor, S. Gariazzo, F. Gatti, C. Gentile, A. Giachero, J. Gudmundsson, Y. Hochberg, Y. Kahn, M. Lisanti, C. Mancini-Terracciano, G. Mangano, L. Marcucci, C. Mariani, J. Martínez, M. Messina, A. Molinero-Vela, E. Monticone, A. Nucciotti, F. Pandolfi, S. Pastor, J. Pedrós, C.P. de los Heros, O. Pisanti, A. Polosa, A. Puiu, Y. Raitses, M. Rajteri, N. Rossi, R. Santorelli, K. Schaeffner, C. Strid, C. Tully, F. Zhao, K. Zurek, A design for an electromagnetic filter for precision energy measurements at the tritium endpoint, Prog. Part. Nucl. Phys. 106 (2019) 120–131.

[43] M.G. Betti, M. Biasotti, A. Boscá, F. Calle, N. Canci, G. Cavoto, C. Chang, A. Cocco, A. Colijn, J. Conrad, N. D'Ambrosio, N.D. Groot, P. de Salas, M. Faverzani, A. Ferella, E. Ferri, P. Garcia-Abia, I. García-Cortés, G.G. Gomez-Tejedor, S. Gariazzo, F. Gatti, C. Gentile, A. Giachero, J. Gudmundsson, Y. Hochberg, Y. Kahn, A. Kievsky, M. Lisanti, C. Mancini-Terracciano, G. Mangano, L. Marcucci, C. Mariani, J. Martínez, M. Messina, A. Molinero-Vela, E. Monticone, A. Moroño, A. Nucciotti, F. Pandolfi, S. Parlati, S. Pastor, J. Pedrós, C.P. de los Heros, O. Pisanti, A. Polosa, A. Puiu, I. Rago, Y. Raitses, M. Rajteri, N. Rossi, I. Rucandio, R. Santorelli, K. Schaeffner, C. Tully, M. Viviani, F. Zhao, K. Zurek, Neutrino physics with the PTOLEMY project: active neutrino properties and the light sterile case, J. Cosmol. Astropart. Phys. 2019 (07) (2019) 047.

[44] A. Apponi, M.G. Betti, M. Borghesi, A. Boyarsky, N. Canci, G. Cavoto, C. Chang, V. Cheianov, Y. Cheipesh, W. Chung, A.G. Cocco, A.P. Colijn, N. D'Ambrosio, N. de Groot, A. Esposito, M. Faverzani, A. Ferella, E. Ferri, L. Ficcadenti, T. Frederico, S. Gariazzo, F. Gatti, C. Gentile, A. Giachero, Y. Hochberg, Y. Kahn, M. Lisanti, G. Mangano, L.E. Marcucci, C. Mariani, M. Marques, G. Menichetti, M. Messina, O. Mikulenko, E. Monticone, A. Nucciotti, D. Orlandi, F. Pandolfi, S. Parlati, C. Pepe, C. Pérez de los Heros, O. Pisanti, M. Polini, A.D. Polosa, A. Puiu, I. Rago, Y. Raitses, M. Rajteri, N. Rossi, K. Rozwadowska, I. Rucandio, A. Ruocco, C.F. Strid, A. Tan, L.K. Teles, V. Tozzini, C.G. Tully, M. Viviani, U. Zeitler, F. Zhao, Heisenberg's uncertainty principle in the PTOLEMY project: a theory update, Phys. Rev. D 106 (2022) 053002.

[45] Y. Ito, H.-J. Qiu, T. Fujita, Y. Tanabe, K. Tanigaki, M. Chen, Bicontinuous nanoporous n-doped graphene for the oxygen reduction reaction, Adv. Mater. 26 (24) (2014) 4145–4150.

[46] Y. Ito, Y. Tanabe, H.-J. Qiu, K. Sugawara, S. Heguri, N.H. Tu, et al., High-quality three-dimensional nanoporous graphene, Angew. Chem. Int. Ed. 53 (19) (2014) 4822–4826.

[47] Y. Ito, W. Cong, T. Fujita, Z. Tang, M. Chen, High catalytic activity of nitrogen and sulfur co-doped nanoporous graphene in the hydrogen evolution reaction, Angew. Chem. Int. Ed. 54 (7) (2015) 2131–2136.

[48] Y. Tanabe, Y. Ito, K. Sugawara, D. Hojo, M. Koshino, T. Fujita, T. Aida, X. Xu, K.K. Huynh, H. Shimotani, T. Adschiri, T. Takahashi, K. Tanigaki, H. Aoki, M. Chen, Electric properties of dirac fermions captured into 3D nanoporous graphene networks, Adv. Mater. 28 (46) (2016) 10304–10310.

[49] Y. Tanabe, Y. Ito, K. Sugawara, M. Koshino, S. Kimura, T. Naito, I. Johnson, T. Takahashi, M. Chen, Dirac fermion kinetics in 3D curved graphene, Adv. Mater. 32 (48) (2020) 2005838.

[50] M.M.S. Abdelnabi, C. Izzo, E. Blundo, M.G. Betti, M. Sbroscia, G. Di Bella, G. Cavoto, A. Polimeni, I. García-Cortés, I. Rucandio, A. Moroño, K. Hu, Y. Ito, C. Mariani, Nanomaterials 11 (1) (2021) 130.

[51] J. Zhou, Q. Wang, Q. Sun, X.S. Chen, Y. Kawazoe, P. Jena, Ferromagnetism in semihydrogenated graphene sheet, Nano Lett. 9 (11) (2009) 3867–3870.

[52] R. Balog, B. Jørgensen, L. Nilsson, M. Andersen, E. Rienks, M. Bianchi, M. Fanetti, E. Lægsgaard, A. Baraldi, S. Lizzit, Z. Sljivancanin, F. Besenbacher, B. Hammer, T.G. Pedersen, P. Hofmann, L. Hornekær, Bandgap opening in graphene induced by patterned hydrogen adsorption, Nat. Mater. 9 (4) (2010) 315–319.

[53] J. Zhou, Q. Sun, How to fabricate a semihydrogenated graphene sheet? A promising strategy explored, Appl. Phys. Lett. 101 (7) (2012) 073114.

[54] G. Savini, A.C. Ferrari, F. Giustino, First-principles prediction of doped graphane as a high-temperature electron-phonon superconductor, Phys. Rev. Lett. 105 (3) (2010) 1–4.

[55] L. Feng, W.X. Zhang, The structure and magnetism of graphone, AIP Adv. 2 (4) (2012) 042138.

[56] F. Buonocore, A. Mosca Conte, N. Lisi, Effects of the substrate on graphone magnetism: a density functional theory study, Phys. E: Low-Dimens. Syst. Nanostructures 78 (2016) 65–72.

[57] L.A. Chernozatonskii, V.A. Demin, D.G. Kvashnin, Fully hydrogenated and fluorinated bigraphenes–diamanes: theoretical and experimental studies, C 7 (1) (2021) 17.

[58] D.K. Samarakoon, X.Q. Wang, Tunable band gap in hydrogenated bilayer graphene, ACS Nano 4 (7) (2010) 4126–4130.

[59] A.R. Muniz, D. Maroudas, Opening and tuning of band gap by the formation of diamond superlattices in twisted bilayer graphene, Phys. Rev. B 86 (7) (2012) 1–11.

[60] P. Giannozzi, S. Baroni, N. Bonini, M. Calandra, R. Car, C. Cavazzoni, D. Ceresoli, G.L. Chiarotti, M. Cococcioni, I. Dabo, A. Dal Corso, S. de Gironcoli, S. Fabris, G. Fratesi, R. Gebauer, U. Gerstmann, C. Gougoussis, A. Kokalj, M. Lazzeri, L. Martin-Samos, N. Marzari, F. Mauri, R. Mazzarello, S. Paolini, A. Pasquarello, L. Paulatto, C. Sbraccia, S. Scandolo, G. Sclauzero, A.P. Seitsonen, A. Smogunov, P. Umari, R.M. Wentzcovitch, QUANTUM ESPRESSO: a modular and open-source software project for quantum simulations of materials, J. Phys.: Condens. Matter 21 (39) (2009) 395502.

[61] P. Giannozzi, O. Andreussi, T. Brumme, O. Bunau, M. Buongiorno Nardelli, M. Calandra, R. Car, C. Cavazzoni, D. Ceresoli, M. Cococcioni, N. Colonna, I. Carnimeo, A. Dal Corso, S. de Gironcoli, P. Delugas, R.A. DiStasio, A. Ferretti, A. Floris, G. Fratesi, G. Fugallo, R. Gebauer, U. Gerstmann, F. Giustino, T. Gorni, J. Jia, M. Kawamura, H.-Y. Ko, A. Kokalj, E. Küçükbenli, M. Lazzeri, M. Marsili, N. Marzari, F. Mauri, N.L. Nguyen, H.-V. Nguyen, A. Otero-de-la Roza, L. Paulatto, S. Poncé, D. Rocca, R. Sabatini, B. Santra, M. Schlipf, A.P. Seitsonen, A. Smogunov, I. Timrov, T. Thonhauser, P. Umari, N. Vast, X. Wu, S. Baroni, Advanced capabilities for materials modelling with quantum ESPRESSO, J. Phys.: Condens. Matter 29 (46) (2017) 465901.

[62] P. Giannozzi, O. Baseggio, P. Bonfà, D. Brunato, R. Car, I. Carnimeo, C. Cavazzoni, S. de Gironcoli, P. Delugas, F. Ferrari Ruffino, A. Ferretti, N. Marzari, I. Timrov, A. Urru, S. Baroni, Quantum ESPRESSO toward the exascale, J. Chem. Phys. 152 (15) (2020) 154105.

[63] L. Triguero, L.G.M. Pettersson, H. Ågren, Calculations of near-edge X-ray-absorption spectra of gas-phase and chemisorbed molecules by means of density-functional and transition-potential theory, Phys. Rev. B 58 (1998) 8097–8110.

[64] G. Avvisati, S. Lisi, P. Gargiani, A. Della Pia, O. De Luca, D. Pacilé, C. Cardoso, D. Varsano, D. Prezzi, A. Ferretti, M.G. Betti, Fepc adsorption on the Moiré superstructure of graphene intercalated with a cobalt layer, J. Phys. Chem. C 121 (3) (2017) 1639–1647.

[65] S. Baroni, S. de Gironcoli, A. Dal Corso, P. Giannozzi, Phonons and related crystal properties from density-functional perturbation theory, Rev. Mod. Phys. 73 (2) (2001) 515–562.

[66] N. Cavani, M. De Corato, A. Ruini, D. Prezzi, E. Molinari, A. Lodi Rizzini, A. Rosi, R. Biagi, V. Corradini, X.-Y. Wang, X. Feng, A. Narita, K. Müllen, V. De Renzi, Vibrational signature of the graphene nanoribbon edge structure from high-resolution electron energy-loss spectroscopy, Nanoscale 12 (2020) 19681–19688.

[67] A. Marini, C. Hogan, M. Grüning, D. Varsano, Yambo: an ab initio tool for excited state calculations, Comp. Phys. Commun. 180 (8) (2009) 1392–1403.

[68] D. Sangalli, A. Ferretti, H. Miranda, C. Attaccalite, I. Marri, E. Cannuccia, P. Melo, M. Marsili, F. Paleari, A. Marrazzo, G. Prandini, P. Bonfà, M.O. Atambo, F. Affinito, M. Palummo, A. Molina-Sánchez, C. Hogan, M. Grüning, D. Varsano, A. Marini, Many-body perturbation theory calculations using the yambo code, J. Phys.: Condens. Matter 31 (32) (2019) 325902.

[69] G. Onida, L. Reining, A. Rubio, Electronic excitations: density-functional versus many-body Green's-function approaches, Rev. Mod. Phys. 74 (2) (2002) 601–659.

[70] F. Sottile, F. Bruneval, A.G. Marinopoulos, L.K. Dash, S. Botti, V. Olevano, N. Vast, A. Rubio, L. Reining, TDDFT from molecules to solids: the role of long-range interactions, Int. J. Quantum Chem. 102 (5) (2005) 684–701.

[71] M. Bonacci, J. Qiao, N. Spallanzani, A. Marrazzo, G. Pizzi, E. Molinari, D. Varsano, A. Ferretti, D. Prezzi, Towards high-throughput many-body perturbation theory: efficient algorithms and automated workflows, npj Comput. Mater. 9 (2023) 74.

[72] A.C. Ferrari, J.C. Meyer, V. Scardaci, C. Casiraghi, M. Lazzeri, F. Mauri, et al., Raman spectrum of graphene and graphene layers, Phys. Rev. Lett. 97 (2006) 187401.

[73] M.G. Betti, E. Blundo, M. De Luca, M. Felici, R. Frisenda, Y. Ito, S. Jeong, D. Marchiani, C. Mariani, A. Polimeni, M. Sbroscia, F. Trequattrini, R. Trotta, Nanomaterials 12 (15) (2022) 2613.

[74] G. D'Acunto, F. Ripanti, P. Postorino, M.G. Betti, M. Scardamaglia, C. Bittencourt, C. Mariani, Channelling and induced defects at ion-bombarded aligned multiwall carbon nanotubes, Carbon 139 (2018) 768–775.

[75] H. Yanagisawa, T. Tanaka, Y. Ishida, M. Matsue, E. Rokuta, S. Otani, C. Oshima, Analysis of phonons in graphene sheets by means of Hreels measurement and ab initio calculation, Surf. Interface Anal. 37 (2) (2005) 133–136.

[76] T. Zecho, A. Güttler, X. Sha, B. Jackson, J. Küppers, Adsorption of hydrogen and deuterium atoms on the (0001) graphite surface, J. Chem. Phys. 117 (18) (2002) 8486–8492.

[77] L. Kyhl, R. Balog, T. Angot, L. Hornekær, R. Bisson, Hydrogenated graphene on Ir(111): a high-resolution electron energy loss spectroscopy study of the vibrational spectrum, Phys. Rev. B 93 (11) (2016) 1–9.

[78] F.C. Bocquet, R. Bisson, J.-M. Themlin, J.-M. Layet, T. Angot, Reversible hydrogenation of deuterium-intercalated quasi-free-standing graphene on SiC(0001), Phys. Rev. B 85 (2012) 201401.

[79] E. Aréou, G. Cartry, J.-M. Layet, T. Angot, Hydrogen-graphite interaction: experimental evidences of an adsorption barrier, J. Chem. Phys. 134 (1) (2011) 014701.

[80] L. Ley, B. Mantel, K. Matura, M. Stammler, K. Janischowsky, J. Ristein, Infrared spectroscopy of C–D vibrational modes on diamond (100) surfaces, Surf. Sci. 427-428 (1999) 245–249.

[81] B.D. Thoms, J.E. Butler, HREELS and LEED of HC(100): the 2 × 1 monohydride dimer row reconstruction, Surf. Sci. 328 (3) (1995) 291–301.

[82] V. Antonov, I. Bashkin, A. Bazhenov, B. Bulychev, V. Fedotov, T. Fursova, A. Kolesnikov, V. Kulakov, R. Lukashev, D. Matveev, M. Sakharov, Y. Shulga, Multilayer graphane synthesized under high hydrogen pressure, Carbon 100 (2016) 465–473.

[83] D. Lin-Vien, N.B. Colthup, W.G. Fateley, J.G. Grasselli, The Handbook of Infrared and Raman Characteristic Frequencies of Organic Molecules, Academic Press, 1991.

[84] E. Cadelano, P.L. Palla, S. Giordano, L. Colombo, Elastic properties of hydrogenated graphene, Phys. Rev. B. 82 (23) (2010) 1–8.

[85] H. Peelaers, A.D. Hernández-Nieves, O. Leenaerts, B. Partoens, F.M. Peeters, Vibrational properties of graphene fluoride and graphane, Appl. Phys. Lett. 98 (5) (2011) 051914.

[86] X.H. Zhou, Y. Huang, X.S. Chen, W. Lu, Density functional theory study of the vibrational properties of hydrogenated graphene, Solid State Commun. 157 (2013) 24–28.

[87] L.F. Huang, T.F. Cao, P.L. Gong, Z. Zeng, Isotope effects on the vibrational, Invar, and Elinvar properties of pristine and hydrogenated graphene, Solid State Commun. 190 (2014) 5–9.

[88] E. Vishnyakova, G. Chen, B.E. Brinson, L.B. Alemany, W.E. Billups, Structural studies of hydrographenes, Acc. Chem. Res. 50 (6) (2017) 1351–1358.

[89] R. Denk, M. Hohage, P. Zeppenfeld, J. Cai, C.A. Pignedoli, H. Söde, R. Fasel, X. Feng, M. Klaus, S. Wang, D. Prezzi, A. Ferretti, A. Ruini, E. Molinari, P. Ruffieux, Exciton–dominated optical response of ultra-narrow graphene nanoribbons, Nat. Commun. 5 (2014) 4253.

[90] D.Y. Qiu, F.H. da Jornada, S.G. Louie, Optical spectrum of MoS_2: many-body effects and diversity of exciton states, Phys. Rev. Lett. 111 (2013) 216805.